nature communications

Article

https://doi.org/10.1038/s41467-025-62016-1

Geopolymerization threatens the persistence of organic carbon associated with iron in anoxic environments

Received: 9 January 2025

Accepted: 8 July 2025

Published online: 21 July 2025

Check for updates

Cheng Zhao[1,2], Yingxun Du[1], Hongwei Wang[1,2], Wenjie Zhou[1,3], Fan Xun[1], Shun Liu[4], Biao Li[1], Xiancai Lu[5], Qinglong L. Wu[1,6], Ke-Qing Xiao[2,7,8] ✉ & Peng Xing[1,8] ✉

The sequestration of organic carbon (OC) through mineral association in soils and sediments is a crucial process that regulates carbon sink dynamics and the global carbon cycle. However, minerals can participate in both abiotic and biotic OC transformations, altering the persistence of mineral-associated OC under anoxic conditions. In this work, we report that synergistic interactions among metal (oxyhydr)oxides, such as iron (Fe), manganese (Mn), and aluminum (Al) drive the polymerization of simple organic molecules into macromolecular geopolymers, increasing their electron transfer capacity by 52–115%. These geopolymers function as electron shuttles, enhancing OC decomposition through microbial dissimilatory iron reduction. This reduces the mean retention time (MRT) of OC bound to active and inert Fe minerals by 51.4 ± 15.6% and 74.1 ± 13.7%, respectively. Future carbon turnover models should explicitly account for the mineral composition, redox fluctuations, and microbial metabolic pathways to advance the understanding of the Earth's carbon sink.

Mineral-associated organic carbon (MAOC), formed through chemical interactions with minerals, is a key form of organic carbon (OC) in soil and sediment, characterized by prolonged turnover times[1–4]. Fe-bound organic carbon (OC–Fe), comprising 39.0 ± 17.1% to 65.2 ± 27.6% of MAOC, plays a vital role in OC accumulation and preservation by forming Fe–organic complexes[2,5]. In oxic conditions, such as surface soil, redox-active metal (oxyhydr)oxides, particularly iron (Fe) and manganese (Mn) oxides, physically isolate OC from oxygen (O_2) and biotic decomposers, limiting its accessibility to oxidative degradation[1,4,6,7]. However, redox-active metal (oxyhydr)oxides can drive the abiotic transformation of OC–Fe (i.e., geopolymerization) under anoxic conditions[6]. In this process, small organic molecules (e.g., reducing sugars and free amino acids) can be transformed into complex aromatic geopolymers (with a molecular weight more than 1000 Da) containing carbonyl, carboxyl, and amino functional groups[6], naturally accompanied by an increase in the redox reactivity of the products[8,9]. It remains unclear whether the enhancement of redox activity in geopolymers significantly impacts the stability of OC–Fe. Moreover, microbial dissimilatory iron reduction (DIR) can counteract the protective role of Fe for OC under anoxic conditions[10]. Critically, redox-active geopolymers may act as electron shuttles, enabling more efficient electron transfer between DIR microbes and

[1]Key Laboratory of Lake and Watershed Science for Water Security, Nanjing Institute of Geography and Limnology, Chinese Academy of Sciences, Nanjing, China. [2]College of Resources and Environment, University of Chinese Academy of Sciences, Beijing, China. [3]School of Civil Engineering, Southeast University, Nanjing, China. [4]Center for the Pan-Third Pole Environment, Lanzhou University, Lanzhou, China. [5]State Key Laboratory for Mineral Deposits Research, School of Earth Sciences and Engineering, Nanjing University, Nanjing, China. [6]Center for Evolution and Conservation Biology, Southern Marine Science and Engineering Guangdong Laboratory (Guangzhou), Guangzhou, China. [7]State Key Laboratory of Regional and Urban Ecology, Research Center for Eco-Environmental Sciences, Chinese Academy of Sciences, Beijing, China. [8]These authors contributed equally: Ke-Qing Xiao, Peng Xing.
✉e-mail: kqxiao@rcees.ac.cn; pxing@niglas.ac.cn

the extracellular Fe(III) minerals. This may intensify the decomposition of OC–Fe and compromise its stability by associating abiotic geopolymerization and biotic dissimilatory iron reduction.

Sediment carbon sinks in inland waters are critical to terrestrial carbon storage and pivotal in long-term carbon sequestration. It is estimated that ~0.12 Pg of carbon is buried annually in inland waters, accounting for nearly 60% of the oceanic carbon burial[11]. Lalonde et al. reported that, on average, 20.5 ± 7.8% of the total organic carbon is directly associated with Fe, with the highest OC-Fe concentrations found in the uppermost sediment layers, where most reactive iron phases accumulate[12]. The overall dissolved oxygen (DO) profile undergoes a more dramatic change at the sediment-water interface. The distribution of DO in the surface sediments below the interface shows a sharp exponential decrease, decaying several millimeters and quickly falling to near zero[13,14]. The availability of reactive minerals could facilitate the processing of OC-Fe in anoxic conditions, potentially compromising the persistence of organic carbon and leading to further conversion of the carbon sink into a source. We speculate that OC-Fe is susceptible to decompose in anoxic sediment through two interconnected mechanisms: (1) synergistic interactions of reactive minerals drive the transformation of labile OC precursors into macromolecular geopolymers with enhanced electron transfer capacity (ETC), and (2) these redox-active geopolymers act as electron shuttles to accelerate microbial DIR, thereby destabilizing OC-Fe pools.

Here we show that minerals play a crucial role in both biotic and abiotic OC transformations, thereby threatening the persistence of mineral-associated OC under anoxic conditions. The surface sediments were sampled from 14 lakes within the Yangtze River's middle and lower reaches. The sequential extraction method was employed to classify sedimentary Fe minerals into active (AM) and inert (IM) fractions, and the characteristics of the associated OC were subsequently analyzed. Microcosm experiments were designed to investigate the catalytic effects of multi-minerals (Fe, Mn, and Al) in geopolymerization under anoxic conditions, and a proportion of OC–Fe (mean 6.3%) was transformed into redox-active substances. We further demonstrated that the geopolymers acted as electron shuttles, enhancing microbial dissimilatory iron reduction, thereby accelerating anaerobic OC decomposition. These processes substantially destabilize OC-Fe associations and undermine the long-term stability of the OC–Fe carbon pool.

Results

Distribution and characteristics of sediment OC–Fe

The sequential extraction of Fe enables the precise differentiation of various Fe minerals, serving as a vital tool for uncovering their diverse roles in the geopolymerization and stabilization of OC. The iron minerals were classified into two categories based on their redox characteristics[15]: active Fe minerals (AM), which included ferrihydrite and magnetite, and inert Fe minerals (IM), primarily composed of Fe minerals bound to silicates. Subsequently, the content and composition of OC associated with each fraction were analyzed. By undertaking a systematic isolation and analysis of each mineral fraction's functional roles, we identified the key mechanisms driving the stabilization and transformation of OC in complex geochemical systems[5].

The total Fe concentrations (TFe) in the sediments ranged from 20.95 to 54.94 g kg^{-1}, with an average of 43.30 ± 8.53 g kg^{-1}. The AM content in lake sediments was notably high, representing ~67.2 ± 2.7% of the TFe, while IM constituted only about one-third of TFe (Fig. 1a). OC–Fe represents a significant portion of the total organic carbon (TOC) in lake sediments, averaging 40.9 ± 21.0% (Fig. 1b). The quantity of OC associated with active ($OC–Fe_{AM}$) and inert Fe minerals ($OC–Fe_{IM}$) is comparable, with both types binding ~50% of the OC–Fe, each averaging 3.06 g kg^{-1} (Fig. 1b). Three-dimensional excitation-emission matrix fluorescence spectroscopy (3DEEM) was employed to identify and characterize the types of OC associated with iron minerals. The results demonstrated that humic acid-like compounds constituted the most prevalent components in $OC–Fe_{AM}$, whereas protein-like compounds represent the primary component of $OC–Fe_{IM}$ in the sediments (Fig. 1c).

The spatial distribution of OC speciation *in suit* sediments (phenolics, polysaccharides, aromatics, aliphatics, carboxylics, lignin derivatives, peptides, and quinone) and their association with Fe and aluminum (Al) oxides were observed by Synchrotron Radiation-based Fourier Transform Infrared spectroscopy (SR-FTIR, Supplementary Fig. 6)[16]. The results demonstrated significantly positive correlations between OC fractions and Fe/Al minerals (Fig. 1d and Supplementary Table 4). In particular, the spatial distributions of Fe oxides (Fe–O) were found to be significantly correlated with phenolics, polysaccharides, and peptides (R^2 = 0.90–0.92 for Lake LG, R^2 = 0.85–0.93 for Lake DH and R^2 = 0.91–0.96 for Lake BD; $p < 0.001$, Fig. 1d). The strongest correlations were observed between Al oxides (Al–O) and phenolics, polysaccharides, aliphatics, and peptides (R^2 = 0.85–0.91 for Lake LG, R^2 = 0.90–0.96 for Lake DH, and R^2 = 0.94–0.96 for Lake BD; $p < 0.001$). This indicates that minerals (Fe–O and Al–O) have a high affinity for phenolics, polysaccharides, and peptides, which is highly consistent with the sequential extraction results (Fig. 1c). It is noteworthy that the distribution of aromatics, lignin derivatives, and quinones, which have traditionally been considered to be closely associated with humus, also exhibits a strong correlation with Fe and Al minerals (R^2 = 0.72–0.88 for Lake LG, R^2 = 0.79–0.90 for Lake DH and R^2 = 0.90–0.94 for Lake BD; $p < 0.001$).

Multi-mineral interactions in the geopolymerization

A microcosm experiment was conducted using an orthogonal experimental design to investigate the impact of minerals on the geopolymerization and redox properties of the products. The selection of mineral combinations and organic molecules was based on observations from field surveys (Fig. 1 and Supplementary Fig. 2). The physicochemical properties of δ-MnO_2, α-Fe_2O_3, and γ-$Al(OH)_3$ were comprehensively characterized before the experiment (Supplementary Notes 2.1). The organic molecules consisted of common constituents, such as glucose and glycine, as well as five phenolic compounds, including catechol, resorcinol, hydroquinone, phloroglucinol, and protocatechuic. The catalytic effects of eight distinct mineral combinations on the geopolymerization of those organic molecules were investigated (Supplementary Table 3). Subsequently, the produced geopolymers were analyzed for their polymerization rates and redox properties.

The results demonstrated that the synthetic effect of α-Fe_2O_3, δ-MnO_2, and γ-$Al(OH)_3$ combination on the geopolymerization of OC was up to one order of magnitude greater than that observed in a catalyst-free control (Fig. 2a). The geopolymerization efficiencies (refers to the percentage increase in the amount of geopolymers produced under mineral catalysis compared to the catalyst-free control) of catechol, resorcinol, hydroquinone, phloroglucinol, and protocatechuic, were 537.4 ± 264.5%, 796.7 ± 246.2%, 620.5 ± 255.7%, 161.8 ± 154.6%, and 748.5 ± 308.4%, respectively. Although the independent effect of γ-$Al(OH)_3$ in the geopolymerization can be negligible, it can significantly enhance the catalytic effects of α-Fe_2O_3 and δ-MnO_2 on OC transformation. Moreover, δ-MnO_2 displayed a more pronounced catalytic effect than α-Fe_2O_3 on catechol, resorcinol, hydroquinone, and protocatechuic transformation (Supplementary Fig. 3). In contrast, α-Fe_2O_3 displayed significantly greater catalytic activity than δ-MnO_2 in the transformation of phloroglucinol (Supplementary Fig. 3). The overall polymerization ratio (defined as the proportion of organic molecules successfully transformed into geopolymers) was ~6.3%, with the highest conversion efficiency observed in the resorcinol group (Supplementary Fig. 4).

Furthermore, the electron transfer capacity of geopolymers, defined as the sum of their electron-accepting and electron-donating

https://doi.org/10.1038/s41467-025-62016-1

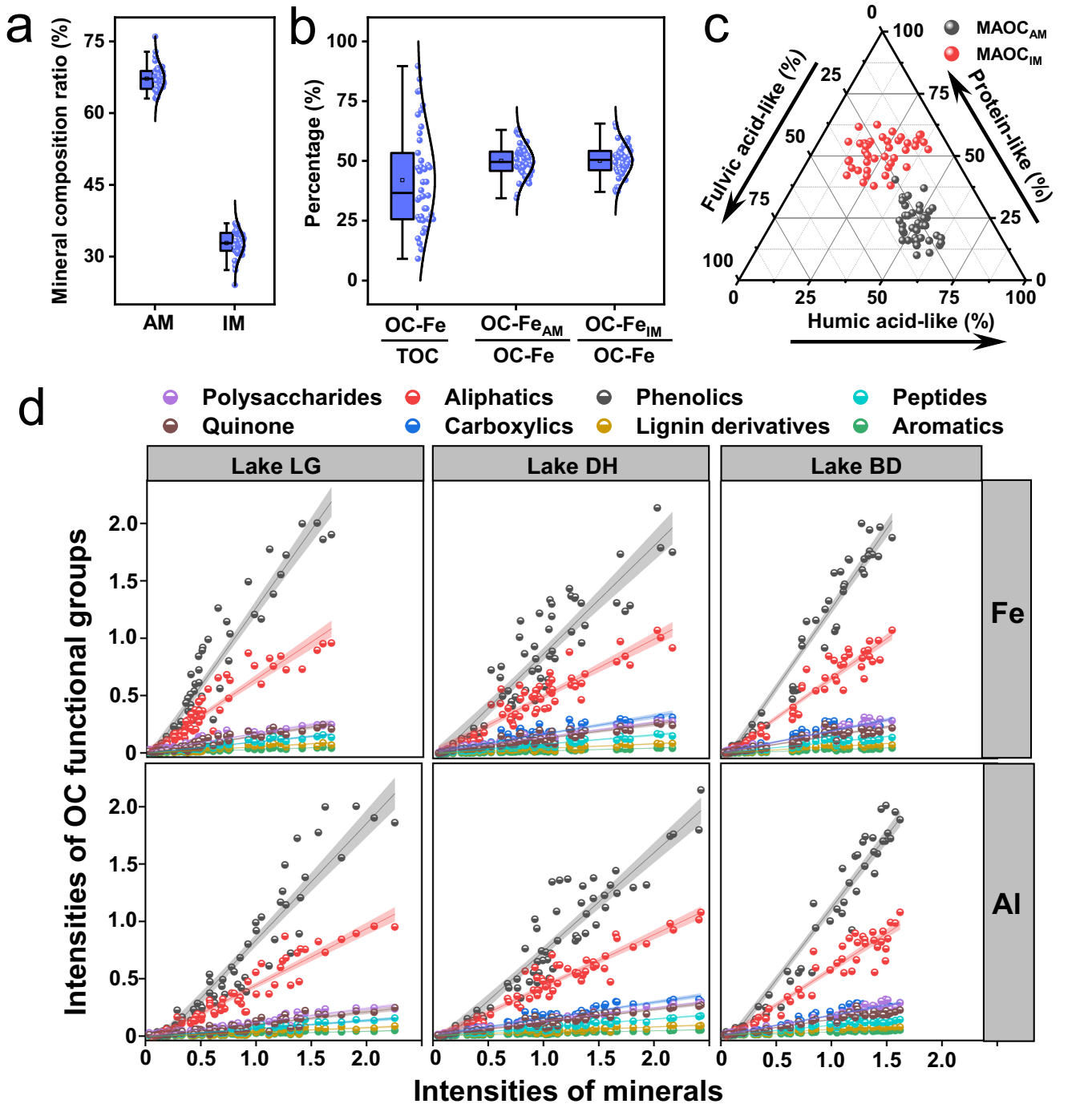

Fig. 1 | The properties of mineral-associated organic carbon (MAOC) in lake sediments. a Distribution of Fe mineral content and forms in the lake sediments, AM: active Fe minerals, IM: inert Fe minerals. Box plots indicate median (middle line), mean (square symbol), 25th, 75th percentile (box), and 1.5 interquartile range (IQR, whiskers) as well as outliers (single points), $n = 42$ independent samples. **b** Proportion of OC–Fe in total sedimentary organic matter, as well as the proportions of OC–Fe associated with active and inert minerals. Box plots indicate median (middle line), mean (square symbol), 25th, 75th percentile (box), and 1.5 interquartile range (IQR, whiskers) as well as outliers (single points), $n = 42$ independent samples. **c** The characteristics of organic matter associated with inert and active Fe minerals by Fluorescence excitation-emission matrices analysis. **d** The scatter plots between the intensity of metal (oxyhydr)oxides (Fe and Al) and OC functional groups in the sediment samples of Lake LG, DH, and BD. Data are presented with points colored by OC functional groups and linear regression lines (solid) fit to the data. Pearson's correlation coefficient (R^2) and corresponding P-values were computed to assess the strength and significance of the linear relationship, with two-sided P values provided in Supplementary Table S4. The confidence bands are 95% sure to contain the best-fit regression line. The SR-FTIR microspectroscopy analysis revealed the presence of several OC functional groups, including phenolics (3379 cm^{-1}), aliphatics (2920 cm^{-1}, 2856 cm^{-1} and 1419 cm^{-1}), carboxylics (1716 cm^{-1} and 1252 cm^{-1}), peptides (1653 cm^{-1}), quinone (1650 cm^{-1}), aromatics (1618 cm^{-1}), lignin derivatives (1515–1513 cm^{-1}), polysaccharides (1036 cm^{-1}), Fe oxides (Fe, 690 cm^{-1}), and Al oxides (Al, 915 cm^{-1}) within the area.

https://doi.org/10.1038/s41467-025-62016-1

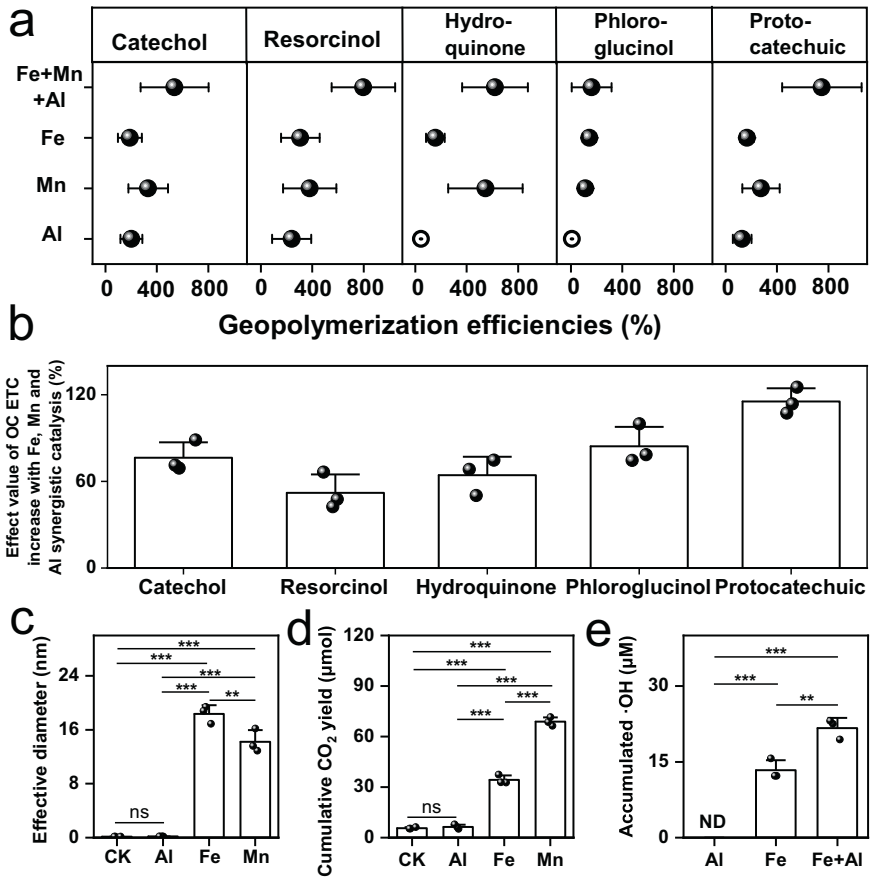

Fig. 2 | The catalysis of α-Fe_2O_3, δ-MnO_2, and γ-$Al(OH)_3$ on geopolymerization of organic molecules. a The efficiencies of geopolymerization are quantified as the mean percentage increase of geopolymers production under mineral catalysis relative to the catalyst-free control. Statistical significance was assessed by two-tailed Student's t-tests comparing each mineral treatment to the control. Solid points represent the statistically significant effects ($p < 0.05$), while hollow points indicate non-significant effects. Error bars represent standard deviation, $n = 3$ independent replicates. **b** The mean percentage increase of the geopolymers' electron transfer capacity (ETC) generated with different phenolic compounds in the Fe + Mn + Al treatment relative to the catalyst-free control. Error bars represent standard deviation, $n = 3$ independent replicates. **c** The mean effective diameter of geopolymers generated with resorcinol as a representative phenolic compound in the Fe, Mn, Al oxides treatments and the catalyst-free control (CK). Error bars represent the standard deviation, $n = 3$ independent replicates. **d** The mean CO_2 production during geopolymerization with resorcinol as a representative phenolic compound in the Fe, Mn, Al oxides treatments and the catalyst-free control (CK). Error bars represent the standard deviation, $n = 3$ independent replicates. **e** The mean generation of free radicals (•OH) with resorcinol as a representative phenolic compound in Fe, Al, and Fe + Al treatments. Error bars represent standard deviation, $n = 3$ independent replicates. ND, not detected. *$p < 0.05$; **$p < 0.01$; *** $p < 0.001$; ns, not significant (ANOVA).

capacities, exhibited a notable increase at the end of the geopolymerization process. On average, geopolymers' electron transfer capacity (ETC) increased by ~78.5 ± 23.9% in the group with Fe, Mn, and Al oxides co-catalysis (Fig. 2b). Moreover, the ETC of geopolymers produced from five phenolic compounds differed by up to twofold, which was highest from protocatechuic (115.4 ± 11.8%) and lowest from resorcinol (52.1 ± 12.5%). In between, the ETC of geopolymers from catechol, hydroquinone, and phloroglucinol were 76.3 ± 10.3%, 64.4 ± 9.8%, and 84.3 ± 15.6%, respectively.

The process of mineral-mediated geopolymerization can be deduced by observing phenomena such as the particle size of the geopolymers and the CO_2 yield during incubation. To illustrate, condensation reactions increase particle size, whereas ring-opening reactions are associated with CO_2 production[17]. Here, we selected resorcinol as a representative phenolic compound. The results demonstrated that the effective diameter of the geopolymer catalyzed by α-Fe_2O_3 was more significant than that of δ-MnO_2 (Fig. 2c). The independent effect of γ-$Al(OH)_3$ on the particle size of the geopolymers can be negligible. This indicated that δ-MnO_2 and α-Fe_2O_3 played a vital role in promoting the polymerization of small molecules. In the meantime, we observed that the reaction can generate a small amount of CO_2, suggesting that mineral catalysis facilitates the cleavage of aromatic rings. The CO_2 yield was significantly higher in δ-MnO_2 and α-Fe_2O_3 treatments than in γ-$Al(OH)_3$ and catalysis-free control (CK) (Fig. 2d). The pro-oxidant role of γ-$Al(OH)_3$ was further elucidated through free radical measurements, which demonstrated that the co-addition of Fe and Al increased ·OH generation by ~62.3% compared to the addition of Fe alone (Fig. 2e).

Footprints of the geopolymerization in lake sediments

The primary components of OC–Fe_{AM} were observed to resemble the characteristics of humic acid-like substances (Fig. 1b), thereby promoting the hypothesis that humic acids (HAs) are the natural products of geopolymerization in lake sediment. Quantification and characterization of sediment HAs were conducted on samples from 14 lakes. The extraction of HAs was performed according to the protocol recommended by the International Humic Substances Society (IHSS). The content of sediment HAs and their ETC characteristics were analyzed for the 14 lakes. The thresholds of the mineral contents were identified according to the nonlinear correlations between the HAs contents and the minerals in lake sediments.

https://doi.org/10.1038/s41467-025-62016-1

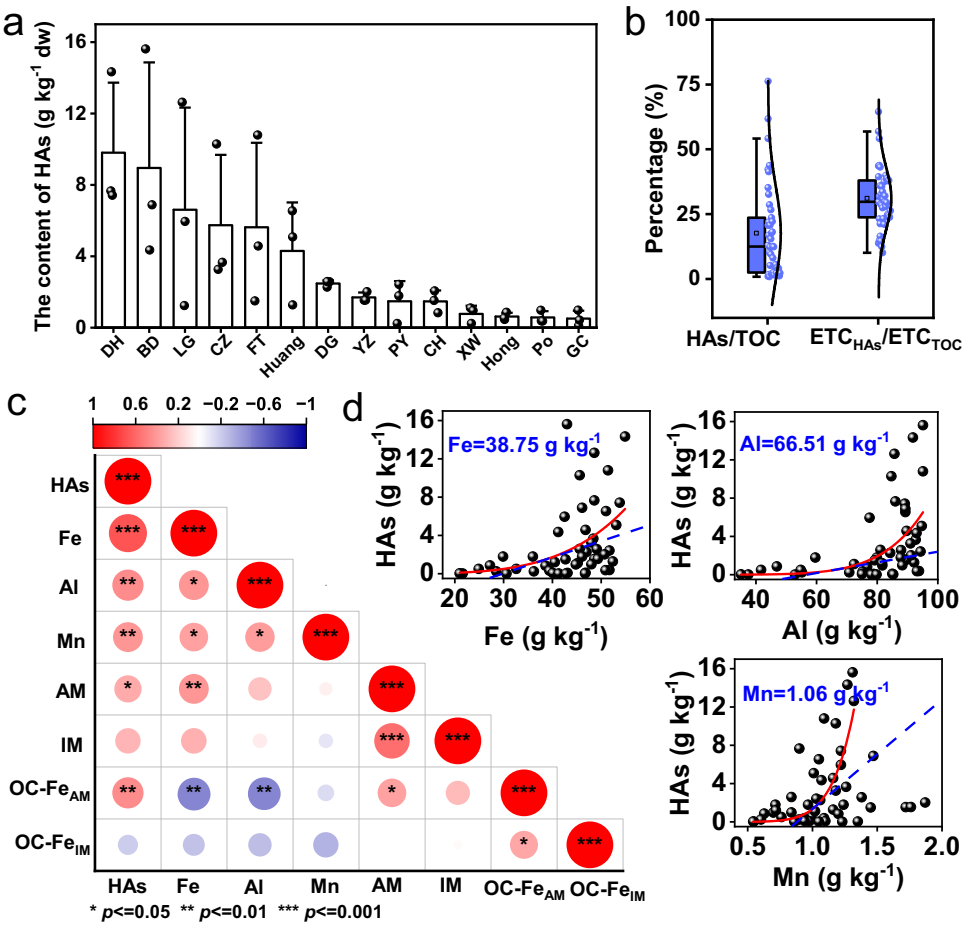

Fig. 3 | The redox-active natural organic matter humic acids (HAs) distribution in lake sediments. a The mean content of HAs in lake sediments. Error bars represent the standard deviation, $n = 3$ independent samples. **b** The proportion of HAs in sediment TOC, and the contribution of HAs' electron transfer capacity (ETC) to the sediment total organic matter's ETC. Box plots indicate median (middle line), mean (square symbol), 25th, 75th percentile (box), and 1.5 interquartile range (IQR, whiskers) as well as outliers (single points), $n = 42$ independent samples. **c** Pearson correlations between contents of Fe, Mn, Al, active Fe minerals (AM), inert Fe minerals (IM), OC–Fe, and HAs. Correlation significance was assessed using two-sided tests. **d** The red solid lines represent the power function fits of the correlation between the mineral contents (Fe, Mn, and Al) and HAs in lake sediments, $n = 42$ independent samples. The tangent line with the most significant slope on the fitted curve was shown in blue dashed. The threshold is the mineral concentration at which the dashed blue line intersects the fitted curve.

As the most significant redox-active substance in sediments, the HAs content exhibited a relatively uniform distribution within a given lake, yet exhibited a high degree of heterogeneity among the 14 lakes (Fig. 3a). The mean concentration of HAs in sediments was ~3.62 g kg^{-1} dw, exhibiting considerable variability (0.51–15.62 g kg^{-1} dw) among lakes. Despite representing only an average of 17.6 ± 18.0% of the sediment TOC, HAs contribute 31.1 ± 11.7% of the sediment organic matter's electron transfer capacity (Fig. 3b). The content of HAs exhibited a significant positive correlation with the AM and OC–Fe_{AM} ($p < 0.05$) but a negative correlation with the OC–Fe_{IM} (not significant, Fig. 3c). It is noteworthy that significant correlations were observed between the concentration of HAs and that of Fe ($R^2 = 0.30$, $p < 0.001$), Al ($R^2 = 0.31$, $p < 0.001$) and Mn ($R^2 = 0.27$, $p < 0.001$, Fig. 3d). The threshold values for Fe, Al, and Mn that promote the formation of HAs are 38.75 g kg^{-1}, 66.51 g kg^{-1}, and 1.06 g kg^{-1}, respectively (Fig. 3d). Fe, Al, and Mn concentrations need to exceed a certain threshold to contribute to the accumulation of HAs. Moreover, the functional group composition of the incubation products is highly analogous to that of natural HAs (Supplementary Fig. 5), thereby providing further corroboration for our hypothesis that geopolymerization represents a crucial pathway for the formation of highly redox-active HAs in sedimentary environments.

Impact of geopolymers on the stability of the OC–Fe carbon pool

The impact of highly redox-active substances generated through mineral-mediated geopolymerization on the anaerobic stability of the OC–Fe carbon pool was examined by incubating surface sediments from each lake for 180 days. The sediments were divided into two groups: untreated sediments (group CK) and sediments receiving an amendment of HAs (group +HAs, extracted from corresponding sediment samples). The mean residence time (MRT) was used as a metric to assess the potential persistence of carbon sinks.

The presence of limited quantities of redox-active substances has been demonstrated to have a significant detrimental impact on the stability of the entire OC–Fe carbon pool. The weighted mean residence time (WMRT) of OC-Fe has been observed to decrease from an average of 1071 days to just 355 days, representing a reduction of ~65.6 ± 12.6% (Fig. 4a). The persistence of OC–Fe_{IM} is significantly higher than that of OC–Fe_{AM}; the average MRTs for OC–Fe_{IM} and OC–Fe_{AM} are 1387.5 days and 766.6 days, respectively. Moreover, the amendment of HAs has a more pronounced effect on the persistence of OC–Fe_{IM}, reducing the average MRT of OC–Fe_{IM} by 74.1 ± 13.7%. The mean MRT of OC–Fe_{AM} was also reduced by 51.4 ± 15.6% (Fig. 4a). At the end of incubation, the abundance of dissimilatory iron reduction bacteria (DIRB) exhibited a 77.1 ± 65.6% increase in HAs-amended

https://doi.org/10.1038/s41467-025-62016-1

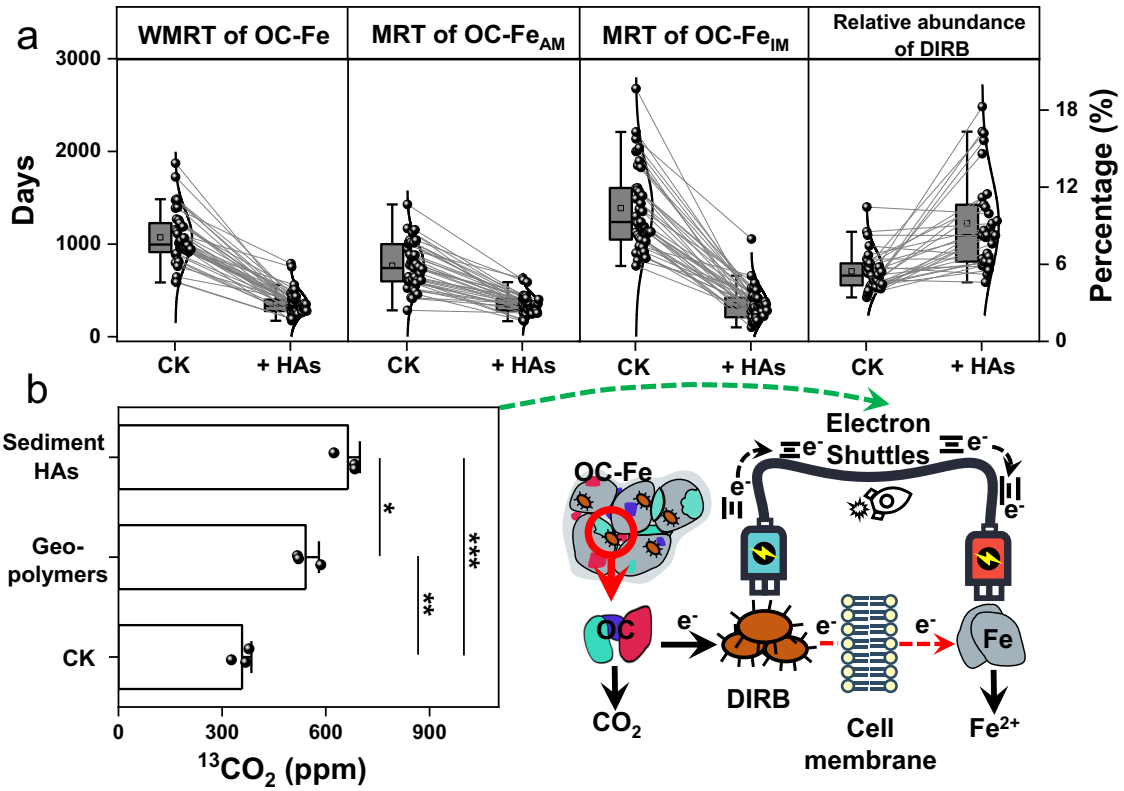

Fig. 4 | Redox-active geopolymers accelerate Fe-bound organic carbon (OC–Fe) decomposition in anoxic conditions by acting as electron shuttles. a The impact of sediment HAs on the weighted average residence time (WMRT) of OC–Fe, the mean residence time (MRT) of OC–Fe$_{IM}$ and OC–Fe$_{IM}$, and the relative abundance of dissimilatory iron reduction bacteria (DIRB). CK: anaerobic incubation of sediment, +HAs: anaerobic incubation of sediment with HAs supplementation. Box plots indicate median (middle line), mean (square symbol), 25th, 75th percentile (box), and 1.5 interquartile range (IQR, whiskers) as well as outliers (single points), $n = 42$ independent samples. The lines are connections between data points. **b** The mean $^{13}CO_2$ production by decomposing $CH_3{}^{13}COOH$ -Fh in the incubation of *Shewanella putrefaciens* BMZ134712 with geopolymers or natural HAs addition. Error bars represent the standard deviation, $n = 3$ independent replicates. $^*p < 0.05$; $^{**}p < 0.01$; $^{***}p < 0.001$; ns, not significant (ANOVA). The schematic diagram illustrates the role of electron shuttles in accelerating electron transfer between the DIR strain and insoluble iron minerals.

sediments compared to blank control sediments (Fig. 4a and Supplementary Fig. 9a). This enriched DIRB abundance aligned with reduced OC–Fe MRT values, indicating redox-active substances' critical role in destabilizing mineral-associated carbon. More detailed results can be found in Supplementary Note 2.2.

To gain further insight into the mechanism by which geopolymers affect OC–Fe stability, we prepared ferrihydrite-bound ^{13}C-labeled acetic acid ($CH_3{}^{13}COOH$-Fh) to simulate OC–Fe and tested its stability by co-culture with a DIR strain (*Shewanella putrefaciens* BMZ134712) and HAs amendment (natural HAs vs experimental geopolymers). The results demonstrated that geopolymers and sediment HAs significantly enhanced $CH_3{}^{13}COOH$-Fh decomposition, with $^{13}CO_2$ yields increasing by 51.5% and 85.4%, respectively (Fig. 4b). Geopolymers with structural characteristics analogous to natural HAs can perform a similar function in anaerobic carbon turnover, acting as electron shuttles to facilitate electron transfer between DIR bacteria and insoluble iron minerals (Fig. 4b). These findings indicate that the redox-active properties generated through the geopolymerization process could pave the way for electron transfer between microorganisms and ambient electron acceptors, thereby accelerating the breakdown of mineral-associated organic carbon.

Discussion

Our findings provide evidence of a "carbon stability dilemma" in anoxic conditions. This was due to the formation of redox-active substances during the multi-mineral catalyzed geopolymerization process, which further stimulated the microbial anaerobic decomposition. This resulted in a net decrease in the overall retention time of the OC–Fe pool. These findings expand the conventional understanding of mineral-mediated carbon stabilization and emphasize the necessity for a more detailed assessment of the influence of mineral-OC interactions and biotic-abiotic interactions on the persistence of the entire carbon pool. A comprehensive reappraisal of mineral- OC interactions and their extensive biogeochemical effects is a critical factor in assessing the overall stability of the OC–Fe carbon pool.

Mineral catalysis plays a pivotal role in enhancing the redox activity of OC, driving the transformation of small molecular compounds (such as proteins and polysaccharides) into redox-active macromolecular structures (geopolymers). A substance's redox activity depends upon the alternating donation and acceptance of electrons by redox-active functional groups, including quinone-like moieties, phenolic hydroxyls, and nitrogen- and sulfur-containing groups[18,19]. Mineral-mediated transformations enhance redox activity by selectively enriching the functional groups through catalytic reactions[9]. Active minerals play a pivotal role in geopolymerization, catalyzing redox processes and improving their reactivity. These transformations occur through the oxidation of OC, including phenols, anilines, and proteins. Active minerals facilitate the cleavage and ring-opening of aromatic compounds, coupled with polycondensation reactions, which transform small molecular compounds into macromolecular organic structures enriched with redox-active moieties[20–22]. These include quinone-like structures. This process is particularly evident in the catalytic roles of Fe and Mn oxides.

Mn oxides, distinguished by their elevated redox activity, demonstrate remarkable efficiency in the cleavage of aromatic rings of OC. This catalytic action results in the opening of aromatic structures, which are then oxidized to form carboxylic groups, undergo decarboxylation, and release CO_2[23]. Mn oxides produce more significant quantities of CO_2 than other minerals, thereby significantly contributing to the breakdown of aromatic rings and enhancing the redox reactivity of the transformed organic matter. In contrast, Fe minerals play an indispensable role in promoting the aggregation and condensation of OC. Due to their natural tendency to concentrate in sedimentary environments, Fe minerals provide a surface that facilitates reactants' orientation and repetitive interaction, reducing their orientational freedom. This structured arrangement increases the efficiency and rate of condensation reactions, promoting the formation of complex macromolecular structures with enhanced electron transfer capacities[7,24]. Aluminum (hydras)oxides, widely distributed in sediments, further complement the transformation processes (Supplementary Fig. 6). Their Brönsted and Lewis acid-base properties enable them to serve as effective adsorbents and catalyst supports[25]. Al minerals create reaction centers and spaces by providing unsaturated coordination sites, thereby facilitating the transformation of OC into carboxyl-rich, low-molecular-weight compounds. Furthermore, Al functions as a pro-oxidant, enabling the generation of free radicals (Fig. 2d), particularly hydroxyl radicals, which are critical in oxidizing OC[26,27]. It has been demonstrated that Fe(II) adsorbed on Al_2O_3 surfaces displays enhanced reductive activity compared to its homogeneous counterpart. This leads to an increase in hydroxyl radical production, which drives OC transformation[28]. The synergistic interaction among metals establishes an interconnected catalytic network where Fe and Mn primarily drive redox transformations. At the same time, Al stabilizes reaction intermediates and extends the reaction space, accelerating OC transformation.

Mineral interactions are a significant factor in the formation of humic substance-like compounds in sediments. In a broader context, the in situ findings from natural sediments highlight the pivotal role of mineral-catalyzed transformations in enhancing the redox reactivity of OC. The positive correlations observed between HAs and active minerals (e.g., Fe, Al, and Mn) in natural sediments are consistent with the microcosm experiments, which suggests that similar mineral-driven processes occur in natural environments. Furthermore, the distribution patterns of HAs across diverse lacustrine systems and their substantial contributions to sedimentary electron transfer capacity reinforce the notion that mineral assemblages play a pivotal role in enhancing the redox reactivity of sedimentary organic matter. These findings not only corroborate the results of the incubation experiment but also underscore the broader environmental implications of the mineral-catalyzed formation of redox-active geopolymers as a critical mechanism in sedimentary systems. In conclusion, it is demonstrated that metal synergistic processing plays an essential role in regulating the redox activity and stability of organic carbon within natural environments.

In lake sediments, approximately half of the OC–Fe is bound to active Fe minerals and available for geopolymerization. The remaining half is physically shielded by inert Fe minerals, preventing microbial assessment and preserving the OC in a readily degradable state. This suggests that OC–Fe may have two potential fates: transformation associated with active minerals (e.g., Fe and Mn) or sequestration in its original form when bound to inert Fe minerals (Fig. 1b). The microcosm incubation experiments reveal that less than 10% of the OC associated with active Fe minerals undergoes polymerization into macromolecular geopolymers (Supplementary Fig. 4). This suggests mineral-mediated geopolymerization modified a relatively minor component of the total OC–Fe carbon pool[6]. Nevertheless, the geopolymers participating in microbial reduction processes may be a primary means of mitigating the instability of mineral-bound organic carbon. The 77.1% increase in DIRB abundance under redox-active substance treatment supports our hypothesis that redox-active geopolymers further accelerate microbial decomposition of OC–Fe, creating an abiotic and biotic synthetic mechanism that undermines carbon stability in anoxic conditions (Supplementary Note 2.2).

$OC–Fe_{IM}$ exhibits significantly greater anaerobic stability than $OC–Fe_{AM}$, with mean residence times of 1387.5 days and 766.6 days, respectively. This difference can be attributed to three main factors: the mechanisms by which the minerals interact with the OC, the distinct characteristics of the mineral types, and their influence on the susceptibility of associated OC to transformation by redox-active substances. For a detailed discussion, refer to the Supplementary Discussion 3.1. Notably, the detrimental impact of redox-active substances is more pronounced on $OC–Fe_{IM}$, where the MRT decreases by ~75%, compared to a 50% reduction for $OC–Fe_{AM}$. This indicates that the instability of $OC–Fe_{IM}$ primarily arises from the electron-shuttling function of redox-active substances rather than being solely attributable to a priming effect. The potential mechanisms by which redox-active substances destabilize $OC–Fe_{IM}$ are discussed (Fig. 5). Initially, $OC–Fe_{IM}$ complexes are stabilized by the physical protection provided by inert Fe minerals, limiting microbial access. However, redox-active substances act as electron shuttles, facilitating extracellular electron transfer (EET) between dissimilatory iron-reducing bacteria and Fe minerals[29]. This electron-shuttling function effectively bypasses the low bioavailability and limited EET efficiency of inert Fe minerals, compromising their protective capacity. As a result, redox-active substances accelerate the microbial decomposition of $OC–Fe_{IM}$, significantly reducing its MRT under anoxic conditions (Fig. 5(i)). Additionally, microbial reduction of Fe may further destabilize $OC–Fe_{IM}$ by disintegrating the $OC–Fe_{IM}$ complexes and releasing previously protected OC[4]. The utilization of easily degradable OC may trigger a priming effect, further promoting the disintegration of $OC–Fe_{IM}$ and the decomposition of OC (Fig. 5(ii)). Abiotic processes involve interactions with reactive minerals, potentially leading to the recombination of OC with active Fe minerals to form new $OC–Fe_{AM}$ complexes (Fig. 5(iii)). These processes highlight the critical role of redox-active substances in destabilizing $OC–Fe_{IM}$.

The results of this study suggest that relying exclusively on iron minerals to guarantee long-term carbon stabilization under anoxic conditions may prove inadequate. The geopolymerization of OC–Fe by active iron minerals can impede the carbon storage process by promoting microbial degradation of OC. This highlights the necessity for a more sophisticated comprehension of carbon sinks, particularly in environments characterized by deoxygenated conditions, such as lake and marine sediments. To ensure the long-term carbon stability of carbon storage, it is essential to consider the influence of mineral processing on carbon retention capacity in deoxygenating environmental conditions, thereby reducing the risk of carbon loss.

Methods

Study sites and sample collection

There are 2,693 lakes larger than 1.0 km^2 in China, with approximately one-quarter located within the middle and lower reaches of the Yangtze River[30,31]. These lakes typically have a shallow depth and a relatively short hydraulic retention time. In recent decades, rapid economic development, high population density, and industrial activity have led to significant terrestrial OC transport, with 75% of the lakes classified as eutrophic or hypertrophic[32]. The abundant OC and mineral substrates in lake sediments provide an ideal system for investigating mineral-mediated OC transformation mechanisms.

This study collected 42 samples from 14 shallow lakes along the middle and lower reaches of the Yangtze River from July to August 2022 (Supplementary Fig. 1 and Supplementary Table 1). Surface sediments (0–5 cm depth) were collected from three representative sites (littoral, transitional, and pelagic zones) in each lake using a

https://doi.org/10.1038/s41467-025-62016-1

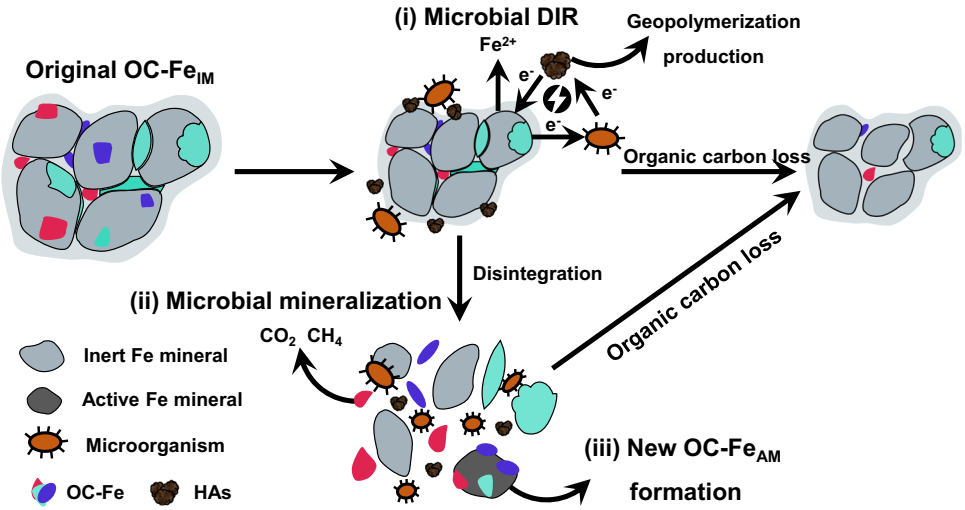

Fig. 5 | The mechanisms influencing the persistence of OC associated with inert Fe mineral (OC–Fe_{IM}) and its transformation under the impact of redox-active substances. OC–Fe_{IM} complexes are primarily stabilized by physical isolation, which reduces OC accessibility to microorganisms. The associated OC often comprises low-molecular-weight compounds that rely on the inert nature of Fe minerals for protection. (i) Redox-active substances act as electron shuttles, facilitating extracellular electron transfer between dissimilatory iron-reducing bacteria and Fe minerals. This process disrupts the physical protection provided by inert Fe minerals, rendering the associated OC more susceptible to microbial attack. The electron-shuttling effect of redox-active substances leads to the reduction of Fe(III) in the OC–Fe_{IM} complexes. This reduction disintegrates the complexes, releasing OC into the surrounding environment. At this stage, the OC is no longer protected and becomes vulnerable to further transformation. Once released, OC undergoes biotic and abiotic transformations. (ii) Biotic processes, driven by microbial activity, can result in the decomposition of OC. (iii) Abiotic processes involve interactions with active Fe minerals, potentially leading to the recombination of OC with active Fe minerals to form new OC–Fe_{AM} complexes. This ultimately reduces the mass of OC–Fe_{IM}.

Peterson grab sampler. Samples from different sites were not mixed and were processed independently to preserve spatial resolution. All samples were immediately transported on ice to the laboratory, where they were divided into two aliquots: one aliquot was stored at 4 °C for subsequent analysis of redox-active substances' impact on OC–Fe stability, while the remaining aliquot was stored at −20 °C for physicochemical characterization of sediments (e.g., Fe, Mn, Al content, and OC composition). Before chemical characterization, sediments were freeze-dried, homogenized, and sieved through a 2 mm mesh to remove coarse debris. The sample pretreatment and chemical analysis details are provided in the Supplementary Methods 1.1.

Extraction and analysis of iron fractions and the associated OC

Sequential extraction was applied to analyze iron and associated OC species in sediment[33–35]. The sequential extraction method, adapted from established protocols for Fe speciation in sediments and soils, was employed to classify sedimentary Fe minerals into active and inert fractions. This approach enables precise differentiation of Fe phases (e.g., ferrihydrite, magnetite, and silicate-bound Fe) based on their redox reactivity and solubility. Briefly, 0.2 g of the freeze-dried sediment samples was sequentially extracted using 1 M $CaCl_2$, 0.5 M HCl, 5 M HCl, and 1.3 M HF with 1.8 M H_2SO_4 to obtain (i) exchangeable iron, (ii) iron in low-crystalline minerals and surface-bound or complexed iron (Fe_{LC}, e.g., ferrihydrite, green rust-like phases and siderite), (iii) highly crystalline iron-bearing minerals (Fe_{HC}, e.g., hematite), and (iv) iron in silicates and clays (inert minerals, IM), respectively. Fe_{LC} and Fe_{HC} are highly active minerals (AM). Details of the experimental procedure are provided in the Supplementary Methods 1.2.

The contents of Fe were measured with a UV–vis spectrometer using the Ferrozine method. The contents of sequentially extractable OC (OC_{Fe}, corresponding to the iron extraction) were measured using a TOC-L CPH (Shimadzu, Japan) total organic carbon analyzer. Fluorescence excitation-emission matrices (EEMs) were used to explore mineral-bound OC's characteristics further. EEM measurements were performed using a fluorescence spectrometer (F-7000, Hitachi High Technologies, Japan) with a 400-voltage xenon lamp at room temperature. Parallel Factor Analysis (PARAFAC) was used to analyze fluorescent EEMs quantitatively[36]. Details of these analyses are included in the Supplementary Methods 1.3 and 1.4.

SR-FTIR microspectroscopy of organic carbon-mineral association in lake sediment

SR-FTIR (synchrotron radiation-based Fourier transform infrared) microspectroscopy was conducted at the BL01B beamline, National Synchrotron Radiation Laboratory (NSRL, Hefei, China)[16] to characterize OC functional groups and their interactions with sediment minerals. Sediment samples (<0.15 mm) suspended in deionized water were air-dried on an aurum window after settling large particles. Spectra were recorded in reflectance mode (4000–650 cm^{-1}, resolution 4 cm^{-1}, 64 scans) and processed using OPUS version 7.5 (Bruker, Germany) for baseline correction. Map profiles of Fe and Al oxides were generated from peak heights at 690 cm^{-1} (Fe–O) and 915 cm^{-1} (Al–O), respectively.

Minerals-catalyzed geopolymerization experiments

Glucose, glycine, and five different types of phenols (catechol, resorcinol, hydroquinone, phloroglucinol, and protocatechuic) were used as representative moieties for polysaccharides, peptides, and phenolics, respectively. The molar concentrations of polysaccharides, peptides, and phenolics in all reactions were 0.05 M, 0.05 M, and 0.1 M (polysaccharides: peptides: phenolics = 1: 1: 2), respectively, as recommended for the polyphenol-Maillard reaction in previous studies[17,37,38]. The effect of minerals on the transformation of OC was studied using an orthogonal test. There were eight different mineral combinations in each phenolic: (1) α-Fe_2O_3 + δ-MnO_2 + γ-$Al(OH)_3$; (2) α-Fe_2O_3 + δ-MnO_2; (3) α-Fe_2O_3 + γ-$Al(OH)_3$; (4) δ-MnO_2 + γ-$Al(OH)_3$; (5) only α-Fe_2O_3; (6) only δ-MnO_2; (7) only γ-$Al(OH)_3$; (8) without mineral (Supplementary Table 3). The minerals used in this study were either laboratory-synthesized or commercially sourced materials, and their

methods of preparation and characterization are described in the Supplementary Methods 1.5.

The concentrations of Fe_2O_3, $Al(OH)_3$, and MnO_2 in all reactions were 1.75 g L^{-1}, 3.5 g L^{-1}, and 0.05 g L^{-1} (Fe: Al: Mn = 35: 70: 1). This ratio was selected to reflect the average composition of in-situ mineral elements in the sediments. After the experimental solutions were prepared, the pH of each experiment was measured and adjusted to pH 7.0 ± 0.2 using either NaOH or HCl buffer solutions. Experiments were conducted on a shaker table in an incubator at 30 °C under strictly anoxic conditions. Before incubation, reaction vessels were purged with high-purity nitrogen gas (N_2) for 30 minutes to remove residual oxygen, and the headspace was maintained under N_2 throughout the experiment. The free radical analysis is described in Supplementary Methods 1.6. The average effective diameter of the geopolymer was determined using the dynamic light scattering (DLS) method, as described in Supplementary Methods 1.7. The measurement of CO_2 production is detailed in Supplementary Methods 1.8.

The concentration of the geopolymerization product was determined using the method described by Moore et al.[6]. Specifically, post-reaction samples were centrifuged at 2800 g for 30 minutes to separate the supernatant from the precipitate. After centrifugation, the precipitate was treated with 0.1 M NaOH overnight under shaking (12 h) to desorb mineral-bound geopolymers[39]. The resulting extract was combined with the original supernatant, and the mixture was dialyzed using a 1000 Da molecular weight cutoff membrane against ultrapure water (18.2 MΩ cm^{-1}) until the conductivity of the external water reached ~18 MΩ cm^{-1}. This dialysis process removed any unreacted precursors while retaining the high-molecular-weight end products. The TOC content of the dialyzed solution was then measured to quantify the concentration of the incubation products. The electron transfer capacity of geopolymers is measured using electrochemical methods[40]. To ensure that the experiments proceeded abiotically, all glassware was acid-washed and autoclaved, and all stock solutions, buffer solutions, and experimental solutions were prepared using autoclaved ultrapure water.

The impact of redox-active substances on the OC–Fe pool

Surface sediments from 14 lakes in the middle and lower reaches of the Yangtze River basin were incubated under anoxic conditions for 180 days to assess the long-term stability of OC–Fe and the impact of redox-active substances on its stability. The sediments were divided into two groups, each with three replicates: a CK group and a +HAs group, where HAs extracted from corresponding sediment samples were added to the incubators. To ensure ecological relevance, ~10% of the natural sedimentary HAs were selected (final concentration 0.2 g L^{-1}), aligning with concentrations used in analogous studies of electron shuttle-mediated iron reduction[41]. For each experiment, 5 g of sediment was placed into a 60 mL amber serum bottle with 10 mL Milli-Q water (1:2, w/v) to simulate sedimentary conditions. The bottles were sealed with butyl rubber stoppers and aluminum caps and then purged with N_2 for 30 minutes to ensure anoxic conditions. Incubations were conducted at 30 °C and pH 7.0 ± 0.2, approximating in situ water temperatures under dark and strictly anoxic conditions. At the end of incubation, a portion of the sediment sample was subjected to sequential extraction to isolate and quantify OC–Fe fractions associated with active and inert Fe minerals. An additional portion of the sediment samples was used for analysis of the dynamics of microbial communities. The specific experimental methods are described in Supplementary Methods 1.9.

To illustrate the mechanisms by which redox-active substances, such as natural HAs and geopolymers, affect the stability of OC-Fe complexes, ferrihydrite-bound ^{13}C-labeled acetic acid ($CH_3{}^{13}COOH$-Fh) was synthesized to simulate OC-Fe complexes. The $CH_3{}^{13}COOH$-Fh was incubated with *Shewanella putrefaciens* BMZ134712 under anoxic conditions. The detailed experimental procedures were shown in Supplementary Methods 1.10.

The stability of OC–Fe was evaluated using a first-order double-exponential decay model[42]:

$$Y(t) = A_1 e^{-k1t} + A_2 e^{-k2t} \quad (1)$$

Where: Y(t) represents the remaining OC–Fe concentration at time t; A_1 and A_2 denote the initial OC content associated with active and inert iron minerals, respectively. k_1 and k_2 are the degradation rate constants for the organic carbon pools associated with active and inert iron minerals. t is the incubation time (days). The mean residence time (MRT) and weighted mean residence time (WMRT) values provided a quantitative measure of the persistence and turnover rates of OC–Fe under anoxic conditions, reflecting the impact of redox-active substances and mineral interactions on OC stability. The mean residence time (MRT) for each pool (i = 1 or 2) is calculated as:

$$MRT_i = 1/k_i \quad (2)$$

Where i represents the index of the OC pool, where i = 1 corresponds to the active iron-associated pool, and i = 2 corresponds to the inert iron-associated pool.

The WMRT of the entire OC–Fe pool was derived as a weighted average of MRT values for both pools:

$$WMRT = (A_1/(A_1 + A_2)) \times MRT_1 + (A_2/(A_1 + A_2)) \times MRT_2 \quad (3)$$

Statistical analysis

Statistical analyses and graphical representations were conducted using OriginPro, Version 2024b (OriginLab Corporation, Northampton, MA, USA.). The Shapiro–Wilk test was employed to assess data normality, and one-way ANOVA was utilized to evaluate variance homogeneity. Linear regression models were used to investigate the associations between minerals and carbon functional groups as determined by synchrotron radiation Fourier-transform infrared (SR-FTIR) microspectroscopy[43]. Pearson's correlation analysis was applied to examine the relationships between the content of HAs and minerals. To identify critical mineral thresholds, piecewise regression analysis was applied to correlate Fe, Al, and Mn concentrations with HAs content across all samples. This statistical method identifies inflection points where the relationship between mineral concentration and HAs content undergoes a sudden shift, indicating a transition in catalytic efficiency. The analysis was implemented in R using the segmented package. All statistical tests were performed with a significance level set at α = 0.05.

Data availability

The sequencing data generated in this study have been deposited in the Sequence Read Archive (SRA) under BioProject accession number PRJNA1276708 and can also be viewed in the NODE database under accession OEP00006271. All other data generated in this study are provided in the Supplementary Information and Source Data file (https://doi.org/10.6084/m9.figshare.29445611).

References

1. Xiao, K. Q. et al. Introducing the soil mineral carbon pump. *Nat. Rev. Earth Environ.* **4**, 135–136 (2023).
2. Jia, N., Li, L., Guo, H. & Xie, M. Important role of Fe oxides in global soil carbon stabilization and stocks. *Nat. Commun.* **15**, 10318 (2024).
3. Hemingway, J. D. et al. Mineral protection regulates long-term global preservation of natural organic carbon. *Nature* **570**, 228–231 (2019).

4. Dong, H. et al. Coupled iron cycling and organic matter transformation across redox interfaces. *Nat. Rev. Earth Environ.* **4**, 659–673 (2023).
5. Ruiz, F. et al. Iron's role in soil organic carbon (de)stabilization in mangroves under land use change. *Nat. Commun.* **15**, 10433 (2024).
6. Moore, O. W. et al. Long-term organic carbon preservation enhanced by iron and manganese. *Nature* **621**, 312–317 (2023).
7. Kleber, M. et al. Dynamic interactions at the mineral–organic matter interface. *Nat. Rev. Earth Environ.* **2**, 402–421 (2021).
8. Zhou, Z. et al. Transformation of natural organic matter in simulated abiotic redox dynamic environments: Impact on Fe cycling. *Environ. Sci. Technol.* **58**, 21604–21616 (2024).
9. Liu, Z., Dai, Y., Zhu, H., Liu, H. & Zhang, J. Effects of additive on formation and electron transfer capacity of humic substances derived from silkworm-excrement compost during composting. *J. Environ. Manag.* **351**, 119673 (2024).
10. Chen, C. M., Hall, S. J., Coward, E. & Thompson, A. Iron-mediated organic matter decomposition in humid soils can counteract protection. *Nat. Commun.* **11**, 2255 (2020).
11. Tranvik, L. J. et al. Lakes and reservoirs as regulators of carbon cycling and climate. *Limnol. Oceanogr.* **54**, 2298–2314 (2009).
12. Lalonde, K., Mucci, A., Ouellet, A. & Gélinas, Y. Preservation of organic matter in sediments promoted by iron. *Nature* **483**, 198–200 (2012).
13. Meijer, L. E. & Avnimelech, Y. On the use of micro-electrodes in fish pond sediments. *Aquacultural Eng.* **21**, 71–83 (1999).
14. Michaud, A. B. & Priscu, J. C. Sediment oxygen consumption in Antarctic subglacial environments. *Limnol. Oceanogr.* **68**, 1557–1566 (2023).
15. Wu, S., Konhauser, K. O., Chen, B. & Huang, L. Reactive mineral sink" drives soil organic matter dynamics and stabilization. *npj Mater. Sustainability* **1**, 3 (2023).
16. Kang, J. et al. Organo–organic interactions dominantly drive soil organic carbon accrual. *Glob. Change Biol.* **30**, e17147 (2024).
17. Zou, J. M., Huang, J. Z., Yue, D. B. & Zhang, H. C. Roles of oxygen and Mn (IV) oxide in abiotic formation of humic substances by oxidative polymerization of polyphenol and amino acid. *Chem. Eng. J.* **393**, 124734 (2020).
18. Zhao, X., Tan, W., Dang, Q., Li, R. & Xi, B. Enhanced biotic contributions to the dechlorination of pentachlorophenol by humus respiration from different compostable environments. *Chem. Eng. J.* **361**, 1565–1575 (2019).
19. Yang, P. et al. Loss and increase of the electron exchange capacity of natural organic matter during its reduction and reoxidation: The role of quinone and nonquinone moieties. *Environ. Sci. Technol.* **56**, 6744–6753 (2022).
20. Stone, A. T. & Morgan, J. J. Reduction and dissolution of manganese(III) and manganese(IV) oxides by organics: 2. Survey of the reactivity of organics. *Environ. Sci. Technol.* **18**, 617–624 (1984).
21. Sunda, W. G. & Kieber, D. J. Oxidation of humic substances by manganese oxides yields low-molecular-weight organic substrates. *Nature* **367**, 62–64 (1994).
22. Ma, D., Wu, J., Yang, P. & Zhu, M. Coupled manganese redox cycling and organic carbon degradation on mineral surfaces. *Environ. Sci. Technol.* **54**, 8801–8810 (2020).
23. Chen, Y. M., Tsao, T. M., Liu, C. C., Huang, P. M. & Wang, M. K. Polymerization of catechin catalyzed by Mn-, Fe- and Al-oxides. *Colloids Surf. B: Biointerfaces* **81**, 217–223 (2010).
24. Duval, S. et al. On the why's and how's of clay minerals' importance in life's emergence. *Appl. Clay Sci.* **195**, 105737 (2020).
25. Axe, K. & Persson, P. Time-dependent surface speciation of oxalate at the water-boehmite (γ-AlOOH) interface: implications for dissolution. *Geochimica et. Cosmochimica Acta* **65**, 4481–4492 (2001).
26. Trusiak, A., Treibergs, L. A., Kling, G. W. & Cory, R. M. The role of iron and reactive oxygen species in the production of CO_2 in arctic soil waters. *Geochimica et. Cosmochimica Acta* **224**, 80–95 (2018).
27. Chorover, J. & Amistadi, M. K. Reaction of forest floor organic matter at goethite, birnessite and smectite surfaces. *Geochimica et. Cosmochimica Acta* **65**, 95–109 (2001).
28. Wen, N. et al. Critical roles of low-molecular-weight organic acid in enhancing hydroxyl radical production by ferrous oxidation on γ-Al_2O_3 mineral surface. *Water Res.* **261**, 122052 (2024).
29. Newman, D. K. & Kolter, R. A role for excreted quinones in extracellular electron transfer. *Nature* **405**, 94–97 (2000).
30. Ma, R. et al. China's lakes at present: Number, area and spatial distribution. *Sci. China Earth Sci.* **54**, 283–289 (2011).
31. Hu, M. et al. A dataset of trophic state index for nation-scale lakes in China from 40-year Landsat observations. *Sci. Data* **11**, 659 (2024).
32. Qin, B., Zhang, Y., Zhu, G. & Gao, G. Eutrophication control of large shallow lakes in China. *Sci. Total Environ.* **881**, 163494 (2023).
33. Chen, N. et al. Active iron phases regulate the abiotic transformation of organic carbon during redox fluctuation cycles of paddy soil. *Environ. Sci. Technol.* **55**, 14281–14293 (2021).
34. Voelz, J. L., Johnson, N. W., Chun, C. L., Arnold, W. A. & Penn, R. L. Quantitative dissolution of environmentally accessible iron residing in iron-rich minerals: a review. *Acs Earth Space Chem.* **3**, 1371–1392 (2019).
35. Poulton, S. W. & Canfield, D. E. Development of a sequential extraction procedure for iron: implications for iron partitioning in continentally derived particulates. *Chem. Geol.* **214**, 209–221 (2005).
36. Stedmon, C. A. & Bro, R. Characterizing dissolved organic matter fluorescence with parallel factor analysis: a tutorial. *Limnol. Oceanogr.: Methods* **6**, 572–579 (2008).
37. Zhang, Y., Yue, D. & Ma, H. Darkening mechanism and kinetics of humification process in catechol-Maillard system. *Chemosphere* **130**, 40–45 (2015).
38. Hardie, A. G., Dynes, J. J., Kozak, L. M. & Huang, P. M. The role of glucose in abiotic humification pathways as catalyzed by birnessite. *J. Mol. Catal. A: Chem.* **308**, 114–126 (2009).
39. Shindo, H. Relative effectiveness of short-range ordered Mn(IV), Fe(III), Al, and Si oxides in the synthesis of humic acids from phenolic compounds. *J. Soil Sci. Plant Nutr.* **38**, 459–465 (1992).
40. Klüpfel, L., Piepenbrock, A., Kappler, A. & Sander, M. Humic substances as fully regenerable electron acceptors in recurrently anoxic environments. *Nat. Geosci.* **7**, 195–200 (2014).
41. Stern, N. et al. Dual role of humic substances as electron donor and shuttle for dissimilatory iron reduction. *Environ. Sci. Technol.* **52**, 5691–5699 (2018).
42. Wang, D. et al. Split N and P addition decreases straw mineralization and the priming effect of a paddy soil: a 100-day incubation experiment. *Biol. Fertil. Soils* **55**, 701–712 (2019).
43. Hernandez-Soriano, M. C. et al. Soil organic carbon stabilization: mapping carbon speciation from intact microaggregates. *Environ. Sci. Technol.* **52**, 12275–12284 (2018).

Acknowledgements

We thank Prof. Dr. Xiaojuan Feng for her excellent advice on improving the manuscript. This work was supported by the National Natural Science Foundation of China (92251304, U2102216, and 31722008), the Science and Technology Planning Project of NIGLAS (NIGLAS2022GS02) and the Youth Innovation Promotion Association of CAS (2014273) to P.X., the Project of Southern Marine Science and Engineering Guangdong Laboratory (GML20220017) to Q.L.W., and the Hundred Talents Program of the Chinese Academy of Sciences to K.X.

Author contributions

P.X., C.Z., and K.X. conceived and designed the experiments. H.W. and B.L. organized the collection of lake sediment samples. C.Z., W.Z., F.X., and S.L. performed the research and analyzed data. C.Z. wrote the original draft. P.X., Y.D., X.L., and K.X. reviewed and revised it. P.X., K.X., and Q.L.W. provided funding acquisition support for the research. All authors discussed the results and commented on the manuscript.

Competing interests

The authors declare no competing interests.

Additional information

Supplementary information The online version contains supplementary material available at https://doi.org/10.1038/s41467-025-62016-1.

Correspondence and requests for materials should be addressed to Ke-Qing Xiao or Peng Xing.

Peer review information *Nature Communications* thanks Ming Jiang and the other, anonymous, reviewer(s) for their contribution to the peer review of this work. A peer review file is available.